Journal of Alloys and Compounds 509 (2011) 9200–9206

Contents lists available at ScienceDirect

Journal of Alloys and Compounds

journal homepage: www.elsevier.com/locate/jallcom

Template-free solvothermal synthesis of size-controlled yttria-stabilized-zirconia hollow spheres

Zhanxia Shu, Xiuling Jiao, Dairong Chen*

Key Laboratory for Special Functional Aggregate Materials of Education Ministry, School of Chemistry and Chemical Engineering, Shandong University, Jinan 250100, PR China

ARTICLE INFO

Article history:
Received 15 March 2011
Received in revised form 28 June 2011
Accepted 28 June 2011
Available online 5 July 2011

Keywords:
Zirconia
Hollow spheres
Template-free
Solvothermal synthesis
Size-controlled

ABSTRACT

Tetragonal yttria-stabilized-zirconia (YSZ) hollow spheres were prepared through a template-free solvothermal method in a homogeneous solution of butanol/acetylacetone or ethanol/acetylacetone with $ZrOCl_2{\cdot}8H_2O$ and $Y(NO_3)_3{\cdot}6H_2O$ as the reaction reagents. The hollow spheres were composed of nanometer-sized particles. The sizes of the hollow spheres could be tuned from 300 nm to 900 nm by changing the concentration of $ZrOCl_2{\cdot}8H_2O$ or altering the solvent. Time-dependent experiments showed that the hollow spheres transformed from amorphous solid spheres composed of nanoparticles. The Ostwald ripening process is proposed to explain the formation of the hollow structures. Er^{3+} doped zirconia (ZrO_2) hollow spheres were also synthesized using the same method. Characteristic emission patterns (515–565 nm) and (640–690 nm) were observed from Er^{3+} doped zirconia hollow spheres with 980 nm excitation.

1. Introduction

Zirconia (ZrO_2), an important functional material in industry, has been widely investigated due to its unique properties, such as low thermal conduction, high melting point, high strength, high ionic conductivity and chemical inertness [1]. At atmospheric pressure, ZrO_2 has three polymorphs-cubic, tetragonal, and monoclinic-depending on the temperature [2]. If larger cations of lower valence (e.g., Y^{3+}) are substituted for Zr^{4+}, the high-temperature structures (cubic and tetragonal) can be stabilized at room temperature because the substitution introduces oxygen vacancies which compensate for the difference in charge [3]. Yttria-stabilized-zirconia (YSZ) is widely used as a catalyst, in oxygen sensors, and as the electrolyte in solid oxide fuel cells, among other applications, because of its excellent properties of low thermal conductivity, high ionic conductivity, high corrosion resistance and high refractive index [4–7]. As to zirconia and doped zirconia materials, many kinds of morphologies have been fabricated, such as nanoparticles [8], nanospheres [9], nanobelts [10], nanowires [11,12], nanotubes [13], flake-like structure [14], mesoporous structures [15], hollow structures [16–19], and etc.

Hollow inorganic spheres have special properties such as low densities, high specific surface areas and excellent permeability, and they have potential applications in catalysis [20], drug-delivery carriers [16,21], nanoreactors [22], drug release [23], etc. The routes to prepare hollow structures involve templates [21,24,25] and template-free methods [26–29]. In previous reports, both templates [30–37] and template-free [38] methods have been applied in the preparation of hollow zirconia spheres. However, most of the synthetic processes are complicated and costly, for example, polystyrene/ZrO_2 [32], carbon/ZrO_2 [30], SiO_2/ZrO_2 [31], and Fe_2O_3/ZrO_2 [17] spheres were firstly prepared, and calcining, alkaline or acid etching was used to remove the hard templates. Also, hollow ZrO_2 microspheres were prepared using yeasts or pollen as bio-template [35–37]. Alternatively, a precursor ($Zr(OH)_4$ or $ZrOC_2O_4$ hollow spheres) was prepared firstly, then ZrO_2 hollow spheres were obtained by calcining [33,38]. Although Li and co-workers [34] have prepared hollow ZrO_2 microspheres with a size in the range of 1.0–2.0 μm through an *in situ* source-template-interface reaction route, the uniformity and size of the hollow zirconia spheres could not be controlled. Therefore, finding a simple method to prepare ZrO_2 hollow spheres with controllable size and excellent uniformity still remains great challenge.

In this paper, we produced uniform YSZ hollow spheres with controlled size (300 nm–900 nm) through a template-free, solvothermal method in an ethanol/butanol-acetylacetone system using $ZrOCl_2{\cdot}8H_2O$ and $Y(NO_3)_3{\cdot}6H_2O$ as the reagents. We also investigated the mechanism of formation of the hollow spheres. Er^{3+} doped zirconia hollow spheres were also prepared, and their up-conversion luminescence properties were studied.

* Corresponding author. Tel.: +86 531 8836 4280; fax: +86 531 8836 4281.
E-mail address: cdr@sdu.edu.cn (D. Chen).

0925-8388/$ – see front matter © 2011 Elsevier B.V. All rights reserved.
doi:10.1016/j.jallcom.2011.06.111

2. Experimental

2.1. Materials

Zirconium (IV) oxychloride octahydrate ($ZrOCl_2{\cdot}8H_2O$, AR, Sinopharm Chemical Reagent Co. Ltd., ≥99.0%), yttrium (II) nitrate hexahydrate ($Y(NO_3)_3{\cdot}6H_2O$, AR, Sinopharm Chemical Reagent Co. Ltd., ≥99.0%), n-butanol ($CH_3(CH_2)_2CH_2OH$, AR, Tianjin Guangcheng Chemical Reagent Co. Ltd., ≥99.0%), acetylacetone ($C_5H_8O_2$, AR, Tianjin Kermel Chemical Reagent Co. Ltd., ≥99.5%) and absolute ethanol (C_2H_5OH, AR, Tianjin Standard Co. Ltd., 99.7%) were used as raw materials without further purification.

2.2. Synthesis and preparation of yttria-stabilized-zirconia hollow spheres

In a typical synthesis, 0.322 g of $ZrOCl_2{\cdot}8H_2O$ and 0.033 g of $Y(NO_3)_3{\cdot}6H_2O$ (molar ratio for Zr/Y = 92:8) were dissolved in a 20.0 mL mixture of n-butanol and acetylacetone (volume ratio = 1:1) under magnetic stirring to form a clear solution. Then the mixture was transferred to a 25 mL Teflon-lined stainless steel autoclave and heated at 65 °C for 4 h, then reacted at 200 °C for 12 h. After that, the autoclave was allowed to cool to room temperature naturally. The product was collected by centrifugation, and washed with anhydrous ethanol 3 times and then dried at 60 °C for 6 h in vacuum.

2.3. Characterization

The X-ray diffraction (XRD) patterns were collected on a Rigaku D/Max 2200PC diffractometer with a graphite monochromator and CuKα radiation (λ = 0.15418 nm). The morphology and microstructure of the products were determined using a field emission scanning electron microscope (FE-SEM, TOSHIBA S4800), TEM (JEM-100CXII) with an accelerating voltage of 80 kV, and high-resolution TEM (HR-TEM, JEOL-2010) with an accelerating voltage of 200 kV. TG analysis was carried out on a Mettler Toledo SDTA851^e thermal gravimetric analyzer at a heating rate of 10 °C/min under air atmosphere. The infrared (IR) spectra were measured on a Nicolet 5DX Fourier transform infrared (FT-IR) spectrometer using KBr pellets for the solid samples and the liquid-membrane method for liquid samples. Elemental analysis (C, H contents) were conducted on a Vario El III elemental analyzer. Room-temperature fluorescence spectra were recorded on a Hitachi F-4500 spectrophotometer equipped with a 150 W Xe-arc lamp at a fixed band-pass of 0.2 nm with a 10 nm excitation slit, 8 nm emission slit and 700 V PMT voltage. The up-conversion emission spectra were measured on a modified Hitachi F-500 spectrophotometer with an external tunable 2 W 980 nm laser as the excitation source in place of the xenon lamp in the spectrometer. Raman spectra were recorded at room temperature using LabRAM HR 800 (HORIBA Jobin Yvon) instrument equipped with a 632.8 nm laser beam.

3. Results and discussion

Fig. 1a shows the XRD pattern of the product. All the diffraction peaks can be indexed to the tetragonal structure of YSZ (JCPDS, No. 48-0224), but the peak broadening, which might be due to the small crystalline size of the product, makes it difficult to distinguish the tetrahedral and cubic phases. Raman technique is more sensitive to phase identification of zirconia, so it is selected to further elucidate the structure. In order to improve the Raman signal, YSZ hollow spheres were annealed at 400 °C for 1 h to remove the surface organics [39], and the XRD pattern of the annealed product hardly changed. As shown in Fig. 1b, the peaks at 145, 261, 315, 460, 638 cm^{-1} can be attributed to the tetragonal zirconia, and no

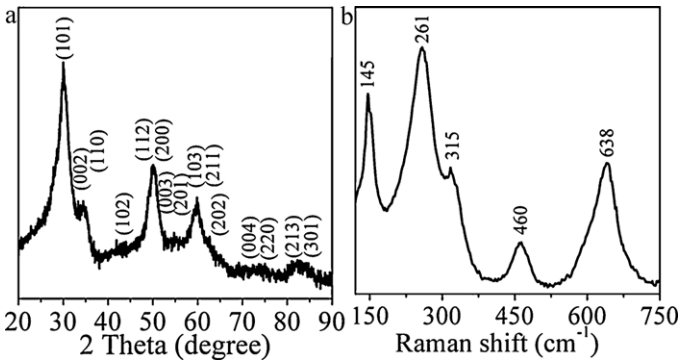

Fig. 1. XRD pattern (a) and Raman spectrum (b) of the YSZ hollow spheres.

peaks for monoclinic and cubic phase are observed [40,41]. The XRD and Raman characterization revealed tetrahedral phase-pure nature of the as-obtained YSZ. From the breadth of the (1 0 1) reflection, the crystallite size calculated using the Scherrer equation is about 3.0 ± 0.2 nm.

Fig. 2a shows the TEM image of the as-synthesized product. The obvious contrast difference between the margin and the center of the particles confirms the existence of hollow structures in the resulting spheres, and the uniformity of the hollow spheres can be seen clearly from the image. The TEM image also demonstrates that the average diameter of the hollow spheres is about 400 nm with shell thickness of ca. 60 nm. The SAED pattern (inset in Fig. 2a) of a single hollow sphere (denoted by the arrow) shows clear diffraction rings, revealing the polycrystalline nature of the hollow sphere. The hollow structure was further investigated by FE-SEM. Fig. 2b indicates that the product is composed of spheres with an average diameter of 400 nm, and a sphere with an aperture could also be observed in the image, confirming that the spheres have hollow interiors. From the surface of the spheres, it can also be observed that the spheres are composed of small particles. The HR-TEM image (Fig. 2c) indicates that the hollow spheres were formed by disoriented aggregation of nanoparticles, which is consistent with the SAED pattern.

The IR spectrum of the YSZ hollow spheres is shown in Fig. 3a. According to the literature [42], the band at 3436 cm^{-1} can be assigned to the asymmetric stretching vibration of OH. The absorptions at 2960, 2929 and 2870 cm^{-1} are assigned to the out-of-plane asymmetric CH_3 stretching vibration, and the symmetric stretching vibrations of C—H in CH_3 appear at 1457 and 1340 cm^{-1}. The strong absorption at 1563 cm^{-1} is ascribed to the stretching vibration of C═O in acetylacetonate. The shift of the C═O vibration compared to pure acetylacetone (1621 cm^{-1}) reveals that the acetylacetone is complexed to Zr^{4+}. The absorptions at 615 and 468 cm^{-1} are due to Zr—O vibrations and the peak at 1026 cm^{-1} to C—O vibrations.

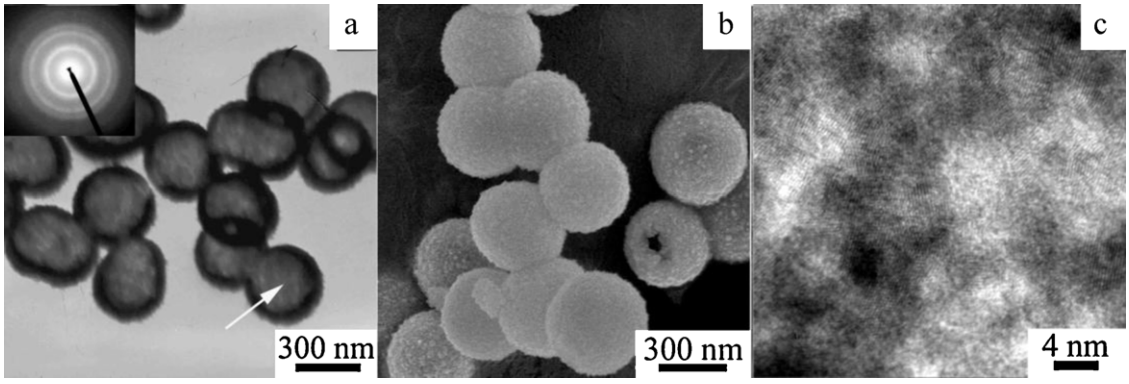

Fig. 2. TEM (a), FE-SEM (b) and HR-TEM (c) images of the YSZ hollow spheres. The inset in (a) is the SAED pattern of the YSZ hollow sphere denoted by the white arrow.

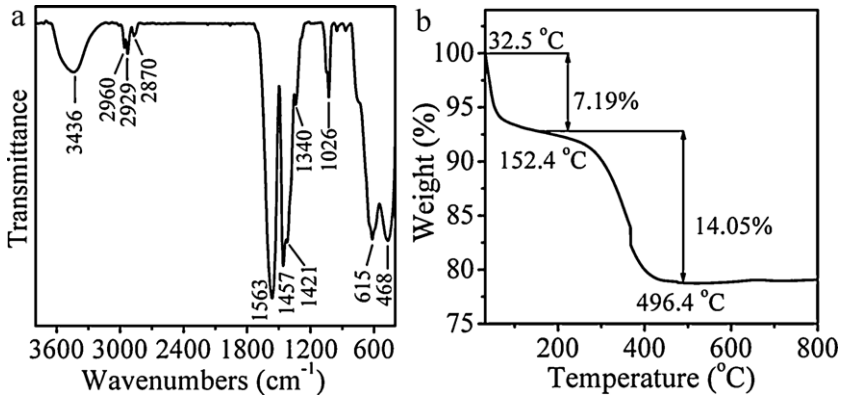

Fig. 3. IR spectrum (a) and TG curve (b) of the YSZ hollow spheres.

Fig. 3b gives the TG curve of the YSZ hollow spheres, and the whole weight loss of ca. 21% can be observed from room temperature to 500 °C. The first drop (up to ~160 °C, 7.19%) is due to desorption of absorbed water, and the second one (160–500 °C, 14.05%) is attributed to the decomposition of the organic materials on the surface of the particles composing the hollow spheres and the loss of water from the hydroxyls. Since the elimination of n-butanol on the particle surfaces should occur from 120 °C to 160 °C, it is concluded based on the IR and TG analyses that the second weight loss step is mainly due to the decomposition of acetylacetone. From the IR and TG analyses of the YSZ hollow spheres, we conclude that there are water molecules, hydroxyls and some coordinated acetylacetone species on the surface of the hollow spheres.

In order to investigate the formation of the hollow structures, a detailed time-dependent experiment was conducted at 200 °C. Fig. 4 gives the TEM images and XRD patterns of the products synthesized at different times. When the solvothermal reaction time is 60 min, there is no solid product, only a yellow solution. When the reaction time is 70 min, solid spheres with broad size distribution from 150 nm to 300 nm are obtained (Fig. 4a). After 2 h, the solid spheres become uniform and larger, ca. 400 nm (Fig. 4b), but their surfaces become coarse as the reaction time increases to 3 h (Fig. 4c). It also can be observed that some spheres combined with each other. After reacting for 4 h, a thin shell is formed outside the shrunken solid spheres (Fig. 4d). The FE-SEM image (inset in Fig. 4d) shows a broken hollow sphere with a core inside, which is consistent with the TEM observation. Further FE-SEM observation (Fig. S1) indicates that some conjoint spheres are detached from each other, which resulted in the aperture of the spheres. At longer reaction times, the inside solid spheres gradually diminish, and the shells of the spheres gradually thicken (Fig. 4e–g). Finally, hollow spheres with a size of ca. 400 nm are formed after a reaction time of 12 h (Fig. 4 g). The XRD patterns (Fig. 4 h) revealed that the solid spheres are amorphous, and the tetragonal-structured zirconia appears with the appearance of the shell. As the reaction time increases from 4 h to 12 h, the crystallinity of the product gradually increases. But when the reaction time is increased beyond 12 h, no obvious changes of the product can be observed.

To further clarify the formation mechanism of the YSZ hollow spheres, IR spectra were taken of the solvents at different points in the reaction process. According to Fig. 5, the IR spectra of the freshly prepared solution, and those treated at 65 °C for 4 h, and at 200 °C for 1 h are almost the same, primarily composed of acetylacetone and n-butanol. After a reaction time of 70 min, the content of acetylacetone significantly reduces, which can be concluded from the decreasing of the characteristic absorption of acetylacetone (1621 cm^{-1}, denoted by the square, SDBS No.1030). At the same time, the characteristic absorption of butyl acetate (1737 cm^{-1}, denoted by the triangle, SDBS No.3292) appears. Extending the reaction time from 70 min to 2 h causes the absorptions of acetylacetone to gradually decrease, accompanied by an enhancement of the absorptions of butyl acetate. Therefore, a reaction occurs between acetylacetone and n-butanol as shown in Eq. (1), which is consistent with that proposed by Adkins et al. [43]. Upon further prolonging the reaction time, no obvious changes can be detected. The organic reaction is basically completed after reacting at 200 °C for 2 h, and this reaction and the formation of the solid spheres occurs at the same time.

$$CH_3\overset{O}{\overset{\|}{C}}CH_2\overset{O}{\overset{\|}{C}}CH_3 + C_4H_9OH \longrightarrow CH_3\overset{O}{\overset{\|}{C}}OC_4H_9 + CH_3\overset{O}{\overset{\|}{C}}CH_3 \quad (1)$$

Table 1 shows the contents of C, H in the products obtained after reacting at 200 °C for 2 h (solid spheres) and 12 h (hollow spheres) and the O contents in the decomposable fraction of the corresponding products. The C contents in the hollow spheres and solid spheres are almost the same, but the H and O contents in the solid spheres are much higher than those in the hollow spheres, suggesting a larger amount of absorbed water.

Comparing the TG analyses of the solid and hollow spheres (Fig. 3b, Fig. 6a, respectively), the evidence also suggests that a relatively larger amount of absorbed water is present in the solid spheres. The TG curve of the solid spheres (Fig. 6a) shows more weight loss than the hollow spheres before 160 °C, and the weight losses after 160 °C are almost the same. The weight gain from 502 °C to 666 °C may be related to the annihilation of surface defects by oxygen [44], and the drop from 666 °C to 800 °C can be attributed to the loss of hydroxyls. It is difficult to determine their precise weight, as the two processes overlap.

Fig. 6b shows the IR spectra of the two samples described in Table 1. The absorptions at 1631 (denoted by the arrow) and 3412 cm^{-1} in the spectrum of the solid spheres belong to the stretching and bending modes of the hydroxyls in the absorbed water, while in the spectrum of the hollow spheres the absorption at 1631 cm^{-1} almost disappears, indicating a decrease of the absorbed water in the hollow spheres. From the results of IR, TG and elemental analyses, it can be concluded that the organic contents in the solid spheres and the hollow spheres are similar, while the solid spheres have more absorbed water.

On the basis of the above experimental results, we believe that Ostwald ripening should be the underlying mechanism for the formation of YSZ hollow spheres. The formation process is proposed as follows. At the beginning, zirconium is chelated with acetylacetone to form zirconium acetylacetonate (Eq. (2)), which can dissolve in

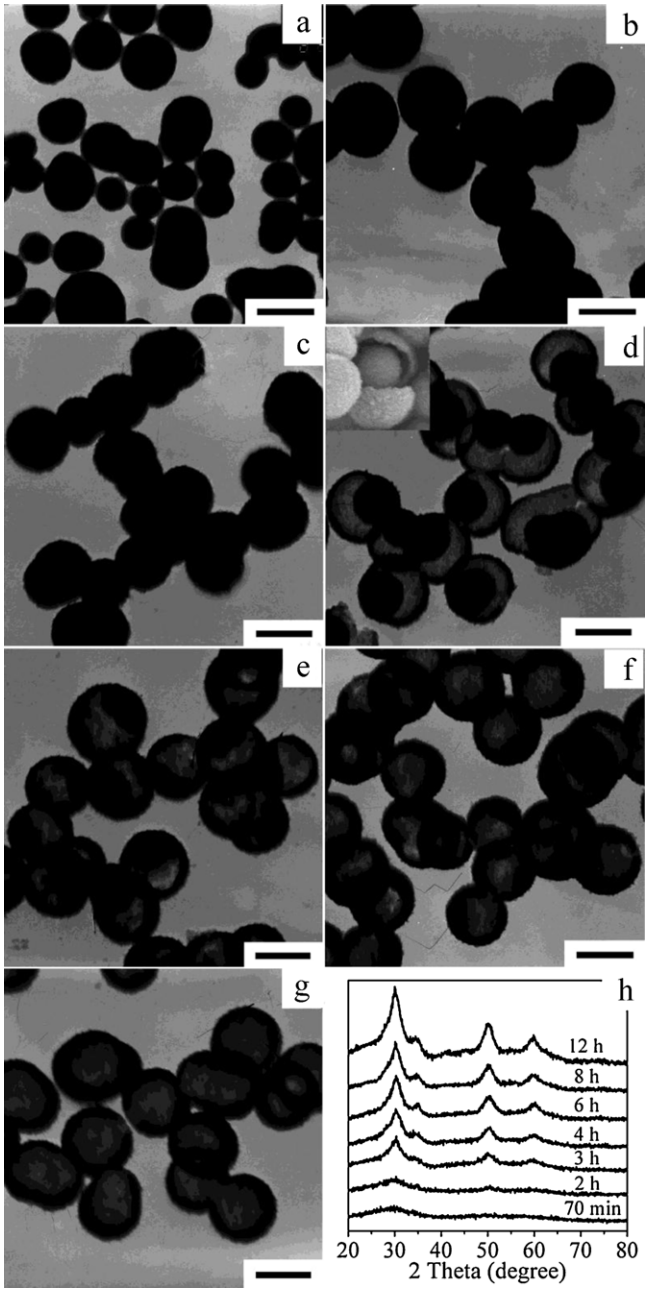

Fig. 4. TEM images (a–g) of samples prepared at different reaction times (200 °C) and the corresponding XRD patterns (h). (a) 70 min, (b) 2 h, (c) 3 h, (d) 4 h, (e) 6 h, (f) 8 h, (g) 12 h. The scale bars in all the images represent 300 nm. The insert in (d) is the FE-SEM image of a broken sphere corresponding to TEM (d).

organic solvents, and there are a few dissociated Zr^{4+} ions in the solution [45].

$$4CH_3\overset{O}{\overset{\|}{C}}CH_2\overset{O}{\overset{\|}{C}}CH_3 + Zr^{4+} \rightleftharpoons Zr(CH_3\overset{O}{\overset{\|}{C}}CH\overset{O}{\overset{\|}{C}}CH_3)_4 + 4H^+ \quad (2)$$

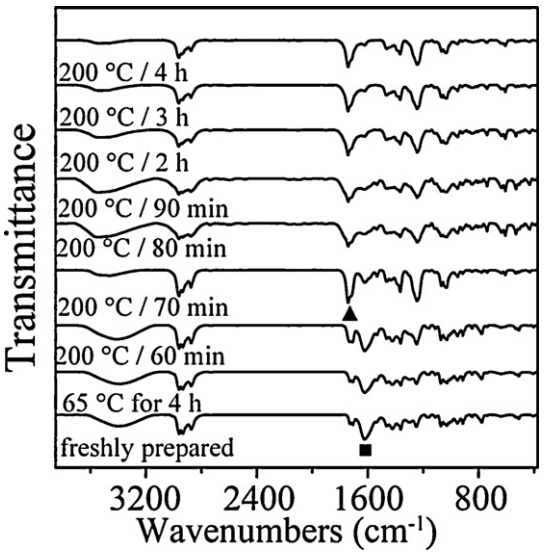

Fig. 5. IR spectra of the filtrate at different points in the procedure.

Then the reaction between the solvents occurs under the solvothermal conditions, i.e. acetylacetone undergoes alcoholysis in n-butanol to produce butyl acetate and acetone, which consumes acetylacetone and makes the reaction shown in Eq. (2) moving to the left, and release Zr^{4+} ions. If the concentration of Zr^{4+} reaches a critical value, Zr^{4+} hydrolyzed to form amorphous solid nanospheres. With the release of Zr^{4+}, the solid spheres gradually grow and spheres as large as 400 nm are formed after almost all the Zr^{4+} is released. As the amorphous solid spheres are surrounded by polar solvents (water and alcohol), the primary particles in the outer surfaces are relatively easy to crystallize. Therefore, less-crystalline particles in the inner region are easy to dissolve [46], and dissolution and recrystallization tend to happen. Then the heterogeneous nucleation of tetragonal YSZ on the solid spheres surface occurs. With the dissolution of the interiors of the amorphous solid spheres, the YSZ shell gradually thickened and the hollow structures formed finally based on an inside-out Ostwald ripening process.

Considering the crystal phase of the zirconia, both the stabilizing effect by Y^{3+}, Mg^{2+}, etc. and the size effect are reported to promote the formation of the tetragonal polymorph [3,47]. Here, Y^{3+} was selected as the stabilizer, and HRTEM observation indicates that the hollow spheres are composed of ca. 3 nm nanoparticles, which are much smaller than the critical size of tetragonal zirconia. To clarify the formation mechanism of the tetragonal zirconia, ZrO_2 hollow spheres were also synthesized under the same conditions but without any stabilizer. As shown in Fig. 7a, all the XRD reflections of the product can be indexed to monoclinic zirconia (JCPDS, No.37-1484). The Raman spectrum (Fig. 7b) also reveals the monoclinic phase-pure nature of the product [40]. The TEM and SEM images (Fig. 8a and b) show the similar morphology and size of the product to the YSZ hollow spheres in the typical synthesis. The SAED pattern (inset in Fig. 8a) of a single hollow sphere shows clear diffraction rings, revealing the polycrystalline nature of the hollow sphere. Further HR-TEM observation (Fig. 8c) revealed that the zirconia hollow spheres are also composed of disoriented

Table 1
Elemental analysis of the samples after reacting at 200 °C for 2 h and 12 h.

Samples	Decomposable fraction (wt%, from TG)	C (wt%)	H (wt%)	O in the decomposable fraction (wt%)	C/H/O (molar ratio)
Solid spheres	29.43	5.629	3.016	20.78	1/6.43/2.77
Hollow spheres	21.24	5.640	1.883	13.72	1/4.01/1.83

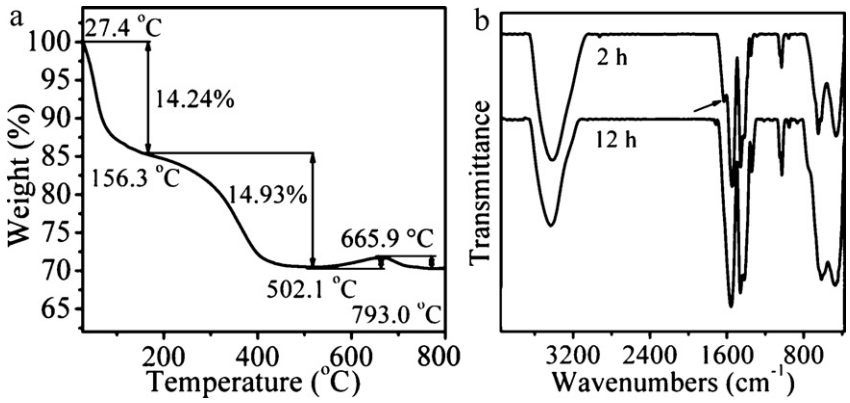

Fig. 6. (a) TG curve of the solid spheres obtained by reacting at 200 °C for 2 h, (b) IR spectra of the products after reaction at 200 °C for different times (2 h and 12 h), the arrow in (b) indicates the newly appeared absorption at 1631 cm^{-1}.

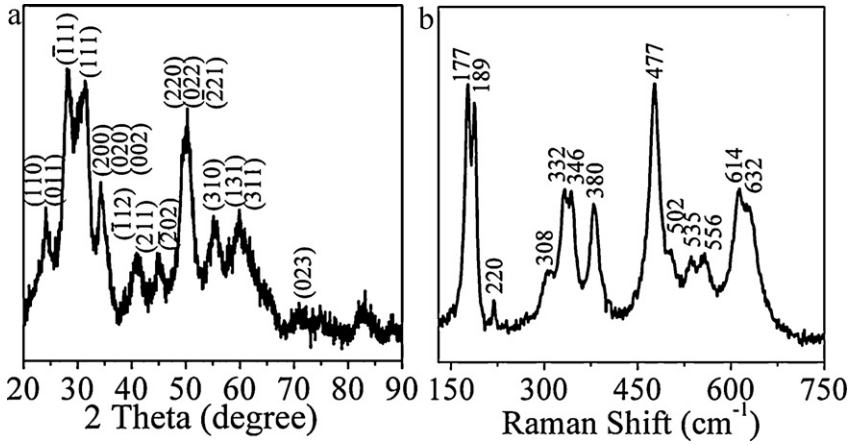

Fig. 7. XRD pattern (a) and Raman spectrum (b) of the ZrO_2 hollow spheres.

aggregated nanoparticles with similar size to that of YSZ hollow spheres. According to the analysis, the crystal phases of the YSZ hollow spheres are dependent on the Y^{3+} stabilizer rather than the size effect. We speculate that the aggregation of the nanoparticles results in a significant decrease of the surface energy, which means the size effect does not control the crystal phase in our system.

By altering the solvent or changing the concentration of $ZrOCl_2{\cdot}8H_2O$ and $Y(NO_3)_3{\cdot}6H_2O$ (keeping the Zr/Y molar ratio at 92:8), the sizes of the hollow spheres can be adjusted from 300 nm to 900 nm, and the shell thickness of the hollow spheres varies between 60 and 150 nm. The SEM images shown in Fig. 9 indicate that all the spheres with different sizes are uniform, and the hollow structures can be clearly seen from the contrast difference on the TEM images and the cracked spheres on the SEM images. If the reaction takes place in a mixture of n-butanol and acetylacetone, hollow spheres with sizes of 300 nm and 400 nm are obtained at $ZrOCl_2{\cdot}8H_2O$ concentrations of 0.0375 mol/L and 0.05 mol/L, respectively (Fig. 9a and b). Using ethanol instead of n-butanol, hollow spheres with sizes of 500 nm, 600 nm, 700 nm, 900 nm are prepared by simply adjusting the concentration of $ZrOCl_2{\cdot}8H_2O$ to 0.0625 mol/L, 0.075 mol/L, 0.0875 mol/L or 0.10 mol/L (Fig. 9c–f). The corresponding XRD patterns reveal that all the products are phase-pure tetragonal YSZ hollow spheres. In the FE-SEM images (Fig. 8b and Fig. 9), some of the hollow spheres with one aperture

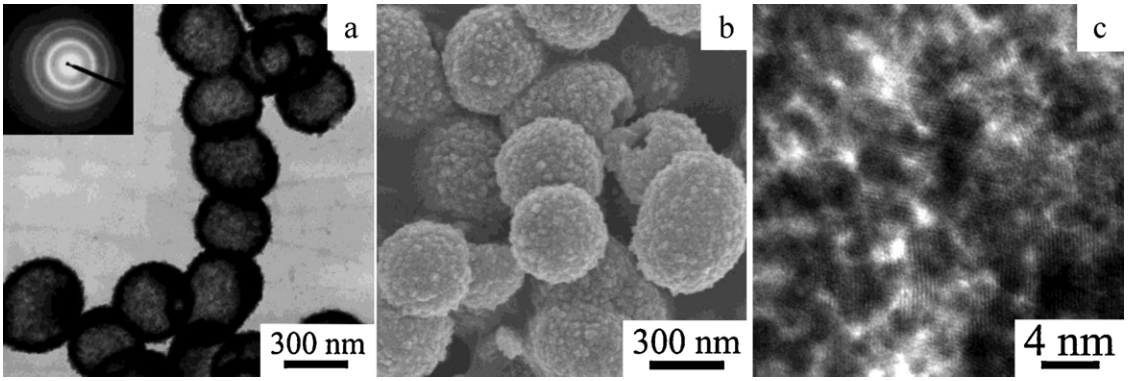

Fig. 8. TEM (a), FE-SEM (b) and HR-TEM (c) images of ZrO_2 hollow nanospheres. The inset in (a) is the SAED patterns of the hollow spheres.

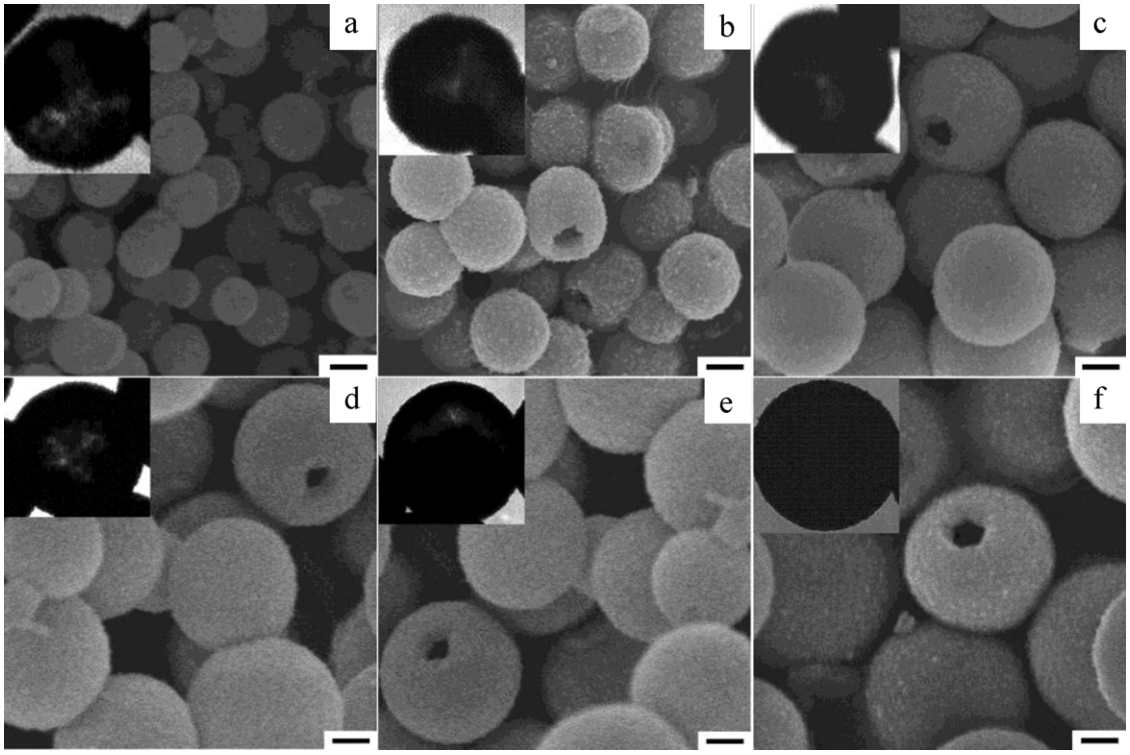

Fig. 9. SEM images of YSZ hollow spheres prepared by altering the solvent or changing the concentration of $ZrOCl_2{\cdot}8H_2O$. (a) n-butanol, 0.0375 mol/L; (b) n-butanol, 0.05 mol/L; (c) ethanol, 0.0625 mol/L; (d) ethanol, 0.075 mol/L; (e) ethanol, 0.0875 mol/L; (f) ethanol, 0.10 mol/L. The scale bars are 200 nm. Insets are the corresponding TEM images.

were observed, which are caused by the departure of one sphere from another.

As described in the above section, the formation of the solid spheres is related to the dissociation of the complex of Zr^{4+} and acetylacetone. In the solution, most of the Zr^{4+} ions are coordinated by acetylacetone. Under solvothermal conditions, Zr^{4+} is released by the reactions between the acetylacetone and the alcohol, and the solid spheres are formed through hydrolysis as soon as the concentration of Zr^{4+} reaches the critical value, then grow larger with the continuous release of Zr^{4+}. With the increasing of the $ZrOCl_2{\cdot}8H_2O$ concentration, more Zr^{4+} would be released during the growth process, and then larger solid spheres are formed, which results in the larger hollow spheres. Different alcohols exhibit different reaction rates with acetylacetone, and then show a slight influence on the size of the spheres.

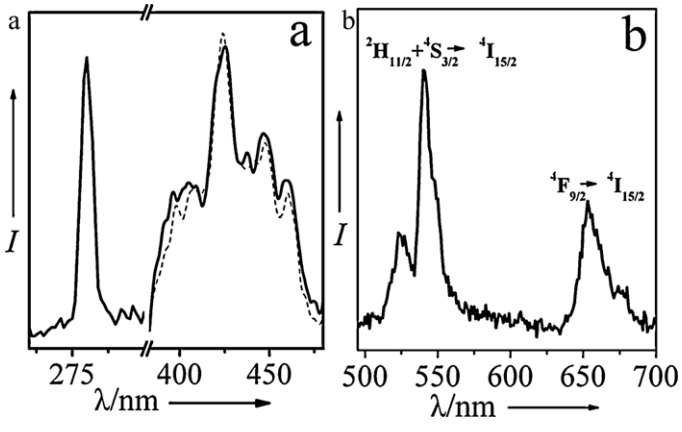

Fig. 10. (a) Room-temperature down-conversion excitation (left) and emission (right) spectra of the YSZ hollow spheres (dash line) and hollow spheres doped with Er^{3+} (solid line). (b) The corresponding up-conversion emission spectrum of the ZrO_2/Er^{3+} hollow spheres. The sample was excited at 980 nm with a 2 W diode laser.

It is reported that Er^{3+} doped zirconia has an up-conversion luminescence property [10]. Here, in addition to YSZ hollow spheres, we synthesized tetragonal zirconia hollow spheres doped with Er^{3+} instead of Y^{3+}. The obtained hollow spheres were calcined in a boat crucible at 800 °C in air for 1 h at a heating rate of 1 °C/min. Both the Y^{3+} and Er^{3+} doped zirconia hollow spheres show almost the same down-conversion emissions (Fig. 10a, excited at 280 nm), which contain a broad band ranging from 380 nm to 480 nm with a maximum at 425 nm. Zr^{4+} itself has no luminescence, so the observed luminescence from ZrO_2 should be related to defects and/or impurities in the system [9], such as the oxygen vacancies induced by the doping of Er^{3+} and Y^{3+} into ZrO_2 hollow spheres [48]. In the up-conversion spectrum of the Er^{3+}-doped hollow spheres (Fig. 10b, excited at 980 nm), characteristic emission patterns (515–565 nm) and (640–690 nm) can be observed, which can be assigned to $^2H_{11/2}+{}^4S_{3/2}\rightarrow{}^4I_{15/2}$ and $^4F_{9/2}\rightarrow{}^4I_{15/2}$ transitions of Er^{3+}, respectively.

4. Conclusions

Yttria-stabilized-zirconia hollow spheres with uniform and adjustable sizes between 300 nm and 900 nm are synthesized by a facile template-free solvothermal strategy. The hollow spheres are produced by initial formation of amorphous solid spheres and then an inside-out Ostwald ripening process. By varying the concentration of the Zr precursor and changing alcohols (ethanol or butanol), YSZ hollow spheres with controllable and uniform size can be prepared, which have potential industrial application. Hollow spheres doped with Er^{3+} show down- and up-conversion luminescence properties, which have value for basic functional optical research and the development of optical devices.

Acknowledgements

This work is supported by the 973 program of the Ministry of Science and Technology of China (no. 2010CB933504) and the Science Funds for Distinguished Young Scientists of Shandong Province (JQ200903). The authors thank Dr. Pamela Holt for proof reading the manuscript.

Appendix A. Supplementary data

Supplementary data associated with this article can be found, in the online version, at doi:10.1016/j.jallcom.2011.06.111.

References

[1] L. Kumari, W.Z. Li, J.M. Xu, R. Leblanc, D.Z. Wang, Y. Li, H.Z. Guo, J.D. Zhang, Cryst. Growth Des. 9 (2009) 3874–3880.
[2] H. Liu, H.R.S. Jazi, M. Bussmann, J. Mostaghimi, Acta Mater. 57 (2009) 6013–6021.
[3] W.C. Jung, J.L. Hertz, H.L. Tuller, Acta Mater. 57 (2009) 1399–1404.
[4] J. Li, N.Q. Zhang, K.N. Sun, W. Sun, W. Li, J. Alloys Compd. 509 (2011) 5388–5393.
[5] P. Vernoux, F. Gaillard, R. Karoum, A. Billard, Appl. Catal. B-Environ. 73 (2007) 73–83.
[6] A. Lari, A. Khodadadi, Y. Mortazavi, Sens. Actuators B-Chem. 139 (2009) 361–368.
[7] Y. An, S.J. Skinner, D.W. McComb, J. Mater. Chem. 20 (2010) 248–254.
[8] R. Dwivedi, A. Maurya, A. Verma, R. Prasad, K.S. Bartwal, J. Alloys Compd. 509 (2011) 6848–6851.
[9] C.M. Zhang, C.X. Li, J. Yang, Z.Y. Cheng, Z.Y. Hou, Y. Fan, J. Lin, Langmuir 25 (2009) 7078–7083.
[10] C.L. Jiang, F. Wang, N.Q. Wu, X.G. Liu, Adv. Mater. 20 (2008) 4826–4829.
[11] W.S. Dong, F.Q. Lin, C.L. Liu, M.Y. Li, J. Colloid Interface Sci. 333 (2009) 734–740.
[12] S.Z. Chu, K. Wada, S. Inoue, H. Segawa, J. Electrochem. Soc. 158 (2011) C148–C157.
[13] L.J. Li, D.X. Yan, J.L. Lei, J.X. He, S.M. Wu, F.S. Pan, Mater. Lett. 65 (2011) 1434–1437.
[14] B.B. Nayak, S.K. Mohanty, M.Q.B. Takmeel, D. Pradhan, A. Mondal, Mater. Lett. 64 (2010) 1909–1911.
[15] H. Zhang, Z.T. An, F. Li, Q. Tang, K. Lu, W.C. Li, J. Alloys Compd. 464 (2008) 569–574.
[16] S.H. Tang, X.Q. Huang, X.L. Chen, N.F. Zheng, Adv. Funct. Mater. 20 (2010) 2442–2447.
[17] C.X. Zhai, N. Du, H. Zhang, D.R. Yang, J. Alloys Compd. (2011), doi:10.1016/j.jallcom.2011.05.073.
[18] X.Z. Zhang, D.R. Fang, B. Lin, Y.C. Dong, G.Y. Meng, X.Q. Liu, J. Alloys Compd. 487 (2009) 631–638.
[19] X.Z. Zhang, B. Lin, Y.H. Ling, Y.C. Dong, D.R. Fang, G.Y. Meng, X.Q. Liu, J. Alloys Compd. 494 (2010) 366–371.
[20] L.X. Xia, H.P. Zhao, G.Y. Liu, X.H. Hu, Y. Liu, J.S. Li, D.H. Yang, X.F. Wang, Colloids Surf. A (2011), doi:10.1016/j.colsurfa.2011.04.016.
[21] Z.H. Xu, P.A. Ma, C.H. Li, Z.Y. Hou, X.F. Zhai, S.S. Huang, J. Lin, Biomaterials 32 (2011) 4161–4173.
[22] G.D. Fu, G.L. Li, K.G. Neoh, E.T. Kang, Prog. Polym. Sci. 36 (2011) 127–167.
[23] C. Zhang, T. Hou, J.F. Chen, L.X. Wen, Particuology 8 (2010) 447–452.
[24] G. Jia, C.M. Zhang, L.Y. Wang, S.W. Ding, H.P. You, J. Alloys Compd. 509 (2011) 6418–6422.
[25] W. Zhou, W.M. Chen, J.W. Nai, P.G. Yin, C.P. Chen, L. Guo, Adv. Funct. Mater. 20 (2010) 3678–3683.
[26] G.Z. Chen, F.F. Zhu, X.A. Sun, S.X. Sun, R.P. Chen, CrystEngComm 13 (2011) 2904–2908.
[27] L.Y. Chen, H. Dai, Y.M. Shen, J.F. Bai, J. Alloys Compd. 491 (2010) L333.
[28] W.C. Li, X.J. Qiao, Q.Y. Zheng, T.L. Zhang, J. Alloys Compd. 509 (2011) 6206–6211.
[29] S. Rengaraj, S. Venkataraj, C.W. Tai, Y. Kim, E. Repo, M. Sillanpaa, Langmuir 27 (2011) 5534–5541.
[30] Y.D. Xia, R. Mokaya, J. Mater. Chem. 15 (2005) 3126–3131.
[31] P.M. Arnal, C. Weidenthaler, F. Schüth, Chem. Mater. 18 (2006) 2733–2739.
[32] D. Chen, J.S. Liu, P. Wang, L. Zhang, J. Ren, F.Q. Tang, W. Wu, Colloids Surf. A 302 (2007) 461–466.
[33] G.R. Duan, A.M. Li, X.J. Yang, L.D. Lu, X. Wang, Microporous Mesoporous Mater. 116 (2008) 86–90.
[34] F.Q. Lin, W.S. Dong, C.L. Liu, Z.T. Liu, M.Y. Li, J. Colloid Interface Sci. 323 (2008) 365–371.
[35] X.H. Yang, X.Q. Song, Y. Wei, W. Wei, L.X. Hou, X.J. Fan, J. Nanosci. Nanotechnol. 11 (2011) 4056–4060.
[36] X.J. Fan, X.Q. Song, X.H. Yang, L.X. Hou, Mater. Res. Bull. 46 (2011) 1315–1319.
[37] X.H. Yang, X.Q. Song, Y. Wei, W. Wei, L.X. Hou, X.J. Fan, Scripta Mater. 64 (2011) 1075–1078.
[38] D. Walsh, L. Arcelli, V. Swinerd, J. Fletcher, S. Mann, B. Palazzo, Chem. Mater. 19 (2007) 503–508.
[39] N.N. Zhao, D.C. Pan, W. Nie, X.L. Ji, J. Am. Chem. Soc. 128 (2006) 10118–10124.
[40] S. Somacescu, J.M.C. Moreno, P. Osiceanu, B.L. Su, V. Parvulescu, J. Phys. Chem. C 114 (2010) 19365–19372.
[41] J.M.C. Moreno, M. Yoshimura, Solid State Ionics 154–155 (2002) 125–133.
[42] R. Di Maggio, R. Campostrini, G. Guella, Chem. Mater. 10 (1998) 3839–3847.
[43] H. Adkins, W. Kutz, D. Coffman, J. Am. Chem. Soc. 52 (1930) 3212–3221.
[44] E.R. Leite, J.A. Cerri, E. Longo, J.A. Varela, C.A. Paskocima, J. Eur. Ceram. Soc. 21 (2001) 669–675.
[45] Z. Holzbecher, L. Divis, M. Kral, Handbook of Organic Reagents in Inorganic Analysis, Halsted Press, New York, 1976, p. 78.
[46] X.W. Lou, Y. Wang, C.L. Yuan, J.Y. Lee, L.A. Archer, Adv. Mater. 18 (2006) 2325–2329.
[47] L.L. Chen, T. Mashimo, E. Omurzak, H. Okudera, C. Iwamoto, A. Yoshiasa, J. Phys. Chem. C 115 (2011) 9370–9375.
[48] H. Nakajima, T. Mori, J. Alloys Compd. 408 (2006) 728–731.